ELSEVIER

Earth and Planetary Science Letters 190 (2001) 125–135

EPSL

www.elsevier.com/locate/epsl

Latent heat effects of the major mantle phase transitions on low-angle subduction

Jeroen van Hunen *, Arie P. van den Berg, Nico J. Vlaar

Department of Theoretical Geophysics, Institute of Earth Sciences, Utrecht University, 3508 TA Utrecht, The Netherlands

Received 18 January 2001; received in revised form 21 May 2001; accepted 21 May 2001

Abstract

Very low to zero shallow dip angles are observed at several moderately young subduction zones with an active trenchward moving overriding plate. We have investigated the effects of latent heat for this situation, where mantle material is pushed through the major mantle phase transitions during shallow low-angle subduction below the overriding plate. The significance of the buoyancy forces, arising from the latent heat effects, on the dynamics of the shallowly subducting slab is examined by numerical modeling. When a 32-Ma-old slab is overridden with 2.5 cm/yr by a continent, flat subduction occurs with a 4–5 cm/yr convergence rate. When latent heat is included in the model, forced downwellings cause a thermal anomaly and consequently thermal and phase buoyancy forces. Under these circumstances, the flat slab segment subducts horizontally about 350 km further and for about 11 Ma longer than in the case without latent heat, before it breaks through the 400-km phase transition. The style of subduction strongly depends on the mantle rheology: increasing the mantle viscosity by one order of magnitude can change the style of subduction from steep to shallow. Similarly, an overriding velocity of less than 1 cm/yr leads to steep subduction, which gradually changes to flat subduction when increasing the overriding velocity. However, these model parameters do not change the aforementioned effect of the latent heat, provided that low-angle subduction occurs. In all models latent heat resulted in a substantial increase of the flat slab length by 300–400 km. Varying the olivine–spinel transition Clapeyron slope γ from 1 to 6 MPa/K reveals a roughly linear relation between γ and the horizontal length of the slab. Based on these results, we conclude that buoyancy forces due to latent heat of phase transitions play an important role in low-angle subduction below an overriding plate.

Keywords: subduction; phase transitions; trenches; migration; buoyancy; viscosity; thermal anomalies

1. Introduction

It has long been recognized that the major mantle phase transitions influence the dynamics of subducting slabs [1–5]. Due to opposing signs of the Clapeyron slopes, cold slabs are accelerated through the 410-km transition, but are retarded or even trapped at the 670-km transition. Latent heat due to these phase transitions gives only a second-order effect, because the cold thermal anomaly of the slab overshadows the temperature change from latent heat release or absorption. During shallow flat subduction, a cold slab does not (initially) penetrate the phase transitions, but instead travels (sub)horizontally. Flat subduction

* Corresponding author. Tel.: +31-30-253-5141.
E-mail address: hunen@geo.uu.nl (J. van Hunen).

0012-821X/01/$ – see front matter
PII: S0012-821X(01)00383-1

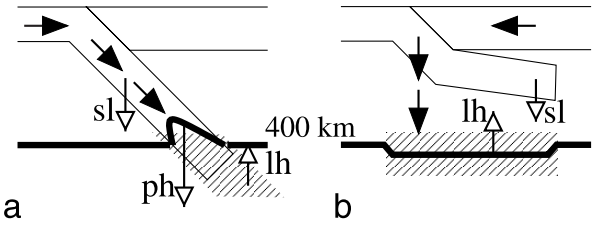

Fig. 1. Schematic representation of the buoyancy effects of latent heat release around 400 km depth during subduction. In the shaded area, the release or advection of latent heat affects the temperature. The thick solid line schematically represents the depth of the 400-km phase transition. Solid arrows denote the flow field, open arrows represent the local buoyancy forces: sl = slab thermal buoyancy, ph = slab phase buoyancy, lh = total latent heat buoyancy. (a) During steep Benioff subduction, the thermal anomaly of the cold slab eclipses the latent heat effect. (b) In case of low-angle subduction below a trenchward moving overriding plate, latent heat release gives a first-order buoyancy effect of the phase transition.

of relatively young oceanic (< 50 Ma) lithosphere is observed in about 10% of the modern subduction zones and is, for example, observed today below the Peru and central Chile [6,7]. In the case of shallow flat subduction below a trenchward moving overriding continent [8,9], relatively warm mantle material below the subducting plate is pushed through the phase transitions. In such a case, latent heat forms a first-order effect of the phase transition, because of the absence of a cold thermal anomaly at the depth of the phase transition. Latent heat release at the 400-km transition results in a temperature rise, which depresses the phase plane to greater depth. The resulting thermal and phase buoyancy will resist further downward motion of mantle material. In this paper, we examine the effects of latent heat under such circumstances. Relevant model parameters are varied to test the robustness of the observed features.

2. Effects of latent heat

When a steeply subducting slab passes the 400-km phase transition, latent heat is released, which heats up the cold slab and reduces its gravitational instability. In general, the temperature rise due to this latent heat release is small: the slab still remains relatively cold (Fig. 1a). However, when material with a very small or absent thermal anomaly passes the phase transition, latent heat results in a first-order buoyancy effect, which may be decisive in maintaining marginal stability in systems with flat subduction. Since the material at the depth of the phase transition is not gravitationally unstable, it must be forced to pass the transition. This is the case when a continent overrides a subducting oceanic plate, by which mechanism the oceanic plate is brought to a depth of at least 100–150 km. This subducting plate, in turn, pushes underlying mantle material down through the phase transitions at greater depths. At the 400-km transition, the released latent heat results in both a thermal buoyancy force and a depression of the equilibrium position of the phase transition, which results in a positive phase buoyancy contribution (Fig. 1b). These buoyancy contributions can influence the dynamics above the transition, since they tend to resist further downwellings. We can make a rough estimation of these effects. The latent heat release per unit mass of mantle material equals [10]:

$$Q_{\mathrm{L}} = \gamma \delta \rho T / \rho^2 \tag{1}$$

where parameters are defined in Table 1. Clapeyron slopes are taken from [11]. Neglecting thermal diffusion, an estimate of the resulting temperature rise is given by $\delta T = Q_{\mathrm{L}}/c_{\mathrm{p}}$, while the phase change equilibrium depression is described by:

$$\delta z = \gamma \delta T / \rho g \tag{2}$$

For a mantle temperature $T = 1728$ K at 400 km depth and parameter values as in Table 1, we obtain a temperature rise $\delta T = 100$ K due to latent heat release. Such a temperature rise would depress the phase transition by approximately $\delta z = 9$ km. We assume a depth increase of all man-

Table 1

Symbol	Meaning	Value used	Dimension	Reference
A	pre-exponential flow law parameter			
	crustal dislocation creep value	8.8×10^{-25}	$Pa^{-n}\ s^{-1}$	
	reference mantle diffusion creep value	1.92×10^{-11}	$Pa^{-n}\ s^{-1}$	[25]
	reference mantle dislocation creep value	2.42×10^{-16}	$Pa^{-n}\ s^{-1}$	[25]
C	Composition parameter	–	–	
c_p	Specific heat	1250	$J\ kg^{-1}\ K^{-1}$	
Di	dissipation number = $\alpha gh/c_p$	0.47	–	
E^*	Activation energy			
	crustal dislocation creep value	260×10^3	$J\ mol^{-1}$	[26]
	reference mantle diffusion creep value	300×10^3	$J\ mol^{-1}$	[25]
	reference mantle dislocation creep value	540×10^3	$J\ mol^{-1}$	[25]
e_{ij}	$e_{ij}=\partial_j u_i+\partial_i u_j$ = strain rate tensor	–	s^{-1}	
H	Non-dimensional radiogenic heat production	–	–	
n	Viscosity stress exponent			
	crustal dislocation creep value	3.4	–	[26]
	reference mantle diffusion creep value	1.0	–	[25]
	reference mantle dislocation creep value	3.5	–	[25]
Q_L	Latent heat release across a phase transition	–	$J\ kg^{-1}$	
R	Gas constant	8.3143	$J\ K^{-1}\ m^{-3}$	
Ra	Thermal Rayleigh number $\rho\alpha\Delta T h^3/\eta\kappa$	1.8×10^7	–	
Rb	Phase Rayleigh number $\delta\rho g h^3/\eta\kappa$			
	400-km phase transition	2.1×10^7	–	
	670-km phase transition	2.4×10^7	–	
Rc	Compositional Rayleigh number $\Delta\rho_c g h^3/\eta\kappa$			
	basalt	3.1×10^7	–	
	harzburgite	6.0×10^6	–	
T	Non-dimensional temperature	–	–	
T_0	Non-dimensional surface temperature	$273/\Delta T$	–	
ΔP	Non-dimensional hydrodynamic pressure	–	–	
ΔT	Temperature contrast across model domain	2300	K	
t	Non-dimensional time	–	–	
$\mathbf{u}$	Non-dimensional velocity $\mathbf{u}=(v,\ w)^T$	–	–	
w	Downward vertical velocity component	–	–	
V^*	Activation volume			
	crustal dislocation creep value	10×10^{-6}	$m^3\ mol^{-1}$	
	reference mantle diffusion creep value	4.5×10^{-6}	$m^3\ mol^{-1}$	
	reference mantle dislocation creep value	14×10^{-6}	$m^3\ mol^{-1}$	[27]
v_0	Overriding velocity (reference model value)	2.5	$cm\ yr^{-1}$	
α	Thermal expansion coefficient	3×10^{-5}	K^{-1}	
Γ_k	Harmonic phase functions for all k mantle phase transitions	–	–	
γ_{400}	Clapeyron slope 400-km phase transition	3	$MPa\ K^{-1}$	[11]
γ_{670}	Clapeyron slope 670-km phase transition	−2.5	$MPa\ K^{-1}$	[11]
$\Delta\rho_c$	Compositional density relative to mantle material		$kg\ m^{-3}$	
	basalt	−400	$kg\ m^{-3}$	
	harzburgite	−77	$kg\ m^{-3}$	
δT	Temperature increase due to latent heat release	–	K	
δz	Phase transition deflection due to latent heat release	–	m	
$\delta\rho_{400}$	Density difference across the 400-km phase transition	273	$kg\ m^{-3}$	[28]
$\delta\rho_{670}$	Density difference across the 670-km phase transition	342	$kg\ m^{-3}$	[28]
η	Non-dimensional viscosity	–	–	
Φ	Non-dimensional viscous dissipation	–	–	
ρ	Mantle density	3416	$kg\ m^{-3}$	
τ_{ij}	Deviatoric stress tensor	–	Pa	
τ	Second invariant of the stress tensor τ_{ij}	–	Pa	

tle material of 100 km due to the overriding effect of a continent of such thickness. Forcing a 100-km-thick vertical column of mantle material with unit cross section through the 400-km transition would reduce its weight relative to a column without vertical movement and would approximately result in a latent heat buoyancy force $F_{lh,400} = 3.4\times10^7$ N/m^2 due to both thermal and phase buoyancy effects of the latent heat release. This estimate of the latent heat effect represents an upper bound for two reasons. First, resistance of mantle downwellings, because the latent heat forces will have a negative feedback on these forces, since less latent heat is released. Second, thermal diffusion will spread the (local) temperature increase, which will diminish the depression of the phase transition.

For comparison, we estimated the thermal and phase buoyancy for a 32-Ma-old slab, before and during the breakthrough at the 400-km transition. We assume a cooling halfspace description of the oceanic lithosphere and vertically integrate the resulting density profile with respect to the mantle adiabat [1] to obtain the negative thermal slab buoyancy F_{sl} of a lithospheric plate just prior to subduction. Assuming the model parameters from Table 1, we obtain $F_{sl} = -4.7\times10^7$ N/m^2, where the minus-sign indicates a downward force. F_{sl} diminishes as the slab heats up during the (sub)-horizontal subduction process. If the slab finally reaches the 400-km transition, the negative phase buoyancy of the uplifted transition within the cold slab will start to contribute. Using $\Delta T = -700$ K in the cold interior of the slab, Eq. 2 would give an uplift of the phase transition of 63 km, and with the parameters from Table 1, this gives a negative phase buoyancy force $F_{ph} = -16.8\times10^7$ N/m^2.

Latent heat is absorbed when material is pushed down through the 670-km phase transition, which gives a negative thermal buoyancy. The phase transition's equilibrium depth, however, is depressed and this gives again a positive phase buoyancy. Thermal and phase buoyancy counteract each-other for this phase transition and the total buoyancy effect of this phase transition will be smaller than that for the 400-km phase transition, but still positive, since the phase buoyancy will be dominant. Applying the same method as for the 400-km phase transition and using a mantle temperature $T = 1908$ K at 670 km depth and parameter values as in Table 1 results in a total positive latent heat buoyancy force $F_{lh,670} = 1.8\times10^7$ N. Comparison of the combined effects of the positive $F_{lh,400}$ and $F_{lh,670}$ with the negative F_{sl} shows that during low-angle subduction below a trenchward moving continent, the total buoyancy effect of the latent heat is of similar magnitude as the negative thermal slab buoyancy. Only if the slab eventually reaches the 400-km transition, the negative F_{ph} will start to dominate the other buoyancy forces, which may result in a flushing event and steeper subduction. How the latent heat would affect the path of the (sub)horizontal slab above the transition is not easily estimated. Vertical motion of the shallow slab and the deeper mantle material around the phase transitions are indirectly coupled by the viscous deformation of intermediate mantle material. Due to the larger distance between slab and transition, the effects of latent heat on shallow flat subduction will be smaller for the 670-km phase transition than for the 400-km phase transition. In order to assess these effects quantitatively, we use numerical modeling and vary the controlling parameters.

3. Model description

The subduction model is based on the extended Boussinesq formulation for an incompressible fluid of infinite Prandtl number [12]. We give a brief description of the governing equations and applied rheology. A more elaborate description is given in [9]. We solve the continuity and momentum equation to obtain the motion of the slab through the mantle below an overriding continent:

$$\partial_j u_j = 0 \tag{3}$$

$$\partial_j(\eta e_{ij}) - \partial_i \Delta P = (RaT - \sum_k Rb_k\Gamma_k + RcC)\delta_{iz} \tag{4}$$

Thermal, compositional, and phase buoyancy, as well as temperature-dependent rheology are accounted for through coupling with the conservation equations for energy and composition:

$$\frac{\partial T}{\partial t} + u_j \partial_j T - Di(T + T_0)w - \sum_k \gamma_k \frac{Rb_k}{Ra} Di(T + T_0)$$

$$\frac{d\Gamma_k}{dt} - \partial_j \partial_j T = \frac{Di}{Ra} \Phi + H \quad (5)$$

$$\frac{\partial C}{\partial t} + u_j \partial_j C = 0 \quad (6)$$

Symbols are defined in Table 1. The buoyancy and latent heat effects of the mantle phase transitions are described by the terms with Γ_k in Eqs. 4 and 5, respectively [12], in a summation of the effects of the 400-km and 670-km phase transitions. Here, we model the subduction of a relatively young lithosphere ($\sim$32 Ma). Based on results from [13,15], we conclude that olivine metastability below the 400-km phase transition is negligible in our model, due to the relatively high slab temperature. Therefore, we do not include olivine metastability in our models. Eqs. 3–5 are solved with a code that is based on the finite element package Sepran [14], which is combined with a Lagrangian tracer particle method to solve Eq. 6. Compositionally, the model distinguishes between two types of mantle material (undepleted lherzolite and depleted harzburgite) and crustal material and each has its own compositional buoyancy, defined through the compositional Rayleigh number *Rc*, as defined in Table 1. For all mantle material, the same composite rheology is applied, which combines both Newtonian and non-Newtonian creep [15,16]. Crustal rheology is described by non-Newtonian creep. Each creep mechanism is prescribed by an Arrhenius relation:

$$e_{ij} = A \tau^{n-1} \tau_{ij} \exp\left[-\frac{E^* + PV^*}{RT}\right] \quad (7)$$

Symbol definition and used reference model values are defined in Table 1. Besides a constant maximum viscosity $\eta_{max} = 10^{23}$ Pa s, an additional stress limiting rheology is applied here, which assumes that material yield when the second invariant of the stress exceeds a pressure-dependent stress limit σ_y [17,18].

We model the subduction process in a Cartesian box of 2000 km deep and 3800 km wide. Our model reference frame is fixed to the overriding continent, such that in this reference frame the subducting plate and underlying mantle move towards this continent. The reference frame of a subduction zone is usually fixed to the deep mantle. For reasons of computational convenience, we model the subduction below a trenchward moving overriding plate in a reference frame that is fixed to this overriding plate: an overriding plate velocity (v_0, 0) is modeled with a no-slip condition at the Earth's surface for the overriding plate and a velocity boundary condition ($-v_0$, 0) at the left hand side and bottom boundaries are imposed. The subducting plate has a free-slip boundary condition, while horizontal flow and a lithostatic pressure are prescribed on the right hand side boundary. Temperature boundary conditions are a mantle adiabat (potential temperature T_p = 1300°C) at the left hand side and bottom boundary, T = 0°C at the surface and a continental geotherm on the right hand side boundary. In between the converging plates, a curved free-slip fault extends to a depth of 100 km. For all model calculations, a single initial situation was created by kinematically driving the subduction of a 32-Ma slab for a duration of 8 Ma, such that the tip of the slab just enters the asthenosphere. After this initial stage, the subduction velocity is no longer prescribed, but driven by internal buoyancy forces in combination with the effects of the overriding plate. The initial mantle has an adiabatic temperature profile below the cool lithospheric plates. Model setup, fault implementation and initial conditions are described in more detail in [9], and the same model parameters are taken, unless explicitly reported.

The effect of a basalt-to-eclogite phase transition in the subducting oceanic crust has been approximated by applying a transition of the compositional buoyancy of crustal material at a depth of 50 km. Temperature dependence of this transition is neglected by setting the Clapeyron slope

to zero. Below the 7-km-thick oceanic crust, an 18-km-thick harzburgitic layer is present. The relative compositional density of basalt and harzburgite with respect to undepleted mantle material in the model are −400 and −77 kg/m^3, respectively. Furthermore, we assume that oceanic compositional buoyancy terms of eclogite and harzburgite cancel each other with respect to undepleted mantle material within a lithospheric column. Therefore, no net compositional buoyancy is applied in our model below 50 km depth. Within the shallow subduction zone, the converging plates are probably decoupled by a fault gouge and a weak basaltic crust. However, for the decoupling of the deeper parts of the two converging plates, several alternative mechanisms have been proposed: eclogite being equally weak as basalt, decoupling within the subducting sediment layers, incomplete dehydration or eclogitization occurring as deep as 250 km [19] or the mantle material overlying the hydrated subducting crust altering to weak serpentinite and talc [20]. To obtain mechanical decoupling between the converging plates, we applied a weak crustal rheology above a depth of 200 km and, for numerical convenience, used the stronger mantle rheology for all materials below this depth. Di-variant mantle phase transitions are included in the model for the 400-km and 670-km discontinuity. These discontinuities are suggested to be as sharp as 4 km [21]. However, as long as the phase transition width is smaller than about 40 km, our model results show little dependence on this width. For numerical convenience, we used a 20-km-wide harmonic parameterization of the phase functions Γ_k for both transitions.

4. Numerical results

For the set of experiments in this section, we

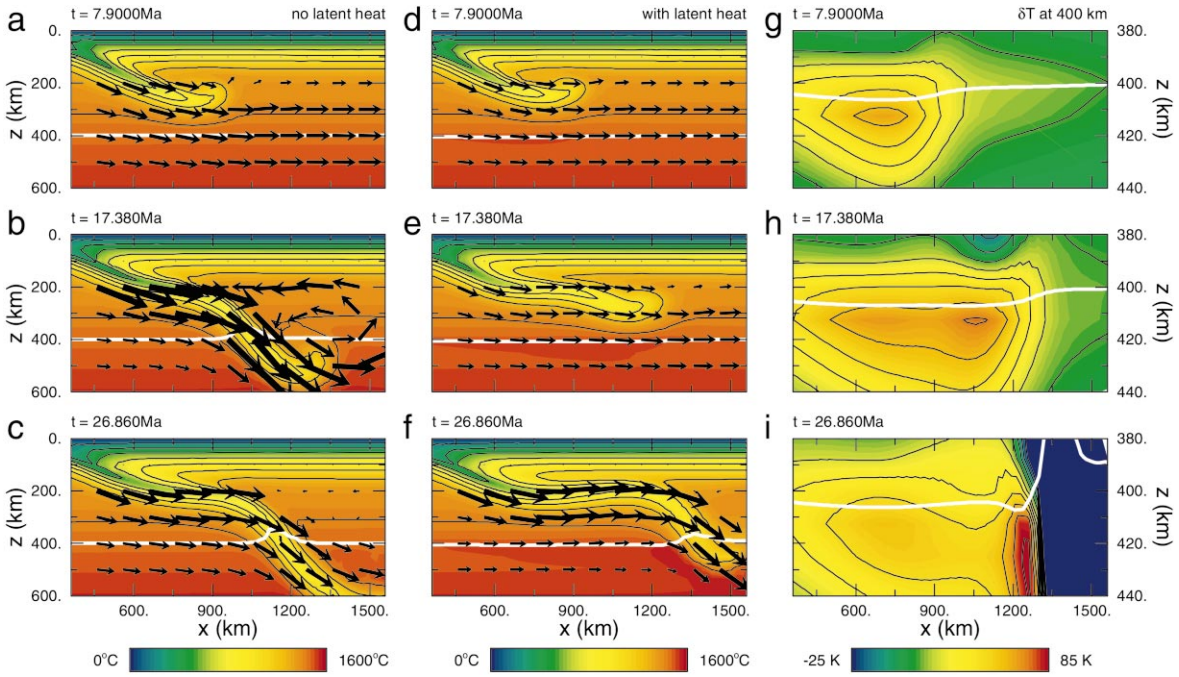

Fig. 2. Temperature contour snapshots of the reference model without (left) and with (middle) latent heat at $t = 7.9$ Ma (a,d), $t = 17.38$ Ma (b,e), and $t = 26.86$ Ma (c,f) are shown. The x-axis displays the horizontal distance to the trench. Black arrows visualize the direction and amplitude of the flow relative to the overriding plate. The horizontal slab length is increased by the effects of latent heat. The right panel shows a vertical exaggeration of the area around the 400-km transition with contour lines of the temperature change with respect to the situation at $t = 0$ Ma. White lines display the 400-km phase transition equilibrium position.

defined a reference model as discussed in Section 3 with reference parameter values as given in Table 1. The effects of latent heat of the two mantle phase transitions on the subduction are investigated. Fig. 2 shows snapshots of the model evolution with and without included latent heat. The results of the model without latent heat (Fig. 2a–c) show a slab which subducts with a small angle and reaches the 400-km phase transition after approximately 14 Ma with an average convergence rate of 4.6 cm/yr. Corresponding results for a model including latent heat (Fig. 2d–f) show a dip angle of the slab reaching zero degrees and a slab traveling horizontally over a longer distance. This slab reaches the transition after approximately 25 Ma with an average convergence rate of 4.1 cm/yr. The black arrows show the direction and amplitude of the mantle flow with respect to the overriding plate. These arrows demonstrate that the breakthrough, which occurs when the slab reaches the 400-km transition, is less vigorous in the model with latent heat. This is due to the extra heating of the slab during its longer route from trench to transition, which reduces the transition uplift. The effects of the latent heat release at the 400-km transition are visualized in Fig. 2g–i, showing the area around 400 km depth with a vertical exaggeration. The plot shows the contours of the temperature field, relative to the situation at $t = 0$ Ma and gives a good impression of the latent heat release due to the overriding plate, together with the resulting (vertical exaggeration of the) phase transition depression.

Fig. 3 shows the effects of the latent heat release/absorption for both phase transitions from the start of the model at $t = 0$ Ma until the moment when the slab reaches the 400-km transition. Fig. 3a gives the maximum temperature change around the transitions with respect to the initial situation, while Fig. 3b shows the corresponding maximum phase equilibrium depressions. Fig. 3a shows a maximum temperature rise of 70–80 K for the 400-km transition, while near the 670-km transition, the temperature drop is only about 20 K. In Fig. 3b, the resulting shift of the equilibrium depth the transitions show a similar trend: the 400-km transition is depressed by 8 km, while the

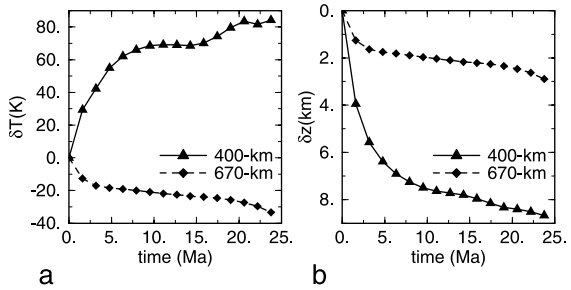

Fig. 3. Evolution of maximum temperature change δT (a) and phase transition depression δz (b) for both mantle phase transitions due to latent heat release/absorption of the downward penetrating mantle material. Both effects are roughly four times larger for the 400-km phase transition than for the 670-km one.

670-km transition shifts only 2–3 km downwards. As expected, these effects are smaller than the ones obtained from the theoretical estimate in Section 2. This is due to the thermal diffusion of the latent heat and a reduced vertical flow from the slab to the transitions, because of the viscous deformation of the mantle in between. The measured perturbations are stronger at the 400-km transition, because it is situated closer to the subducting plate. Furthermore, the influence of the slab on the 670-km transition is partly shielded off by the 400-km transition, which results in a larger flux of mantle material through the 400-km transition. After 10 to approximately 15 Ma, the maximum temperature rise due to the latent heat release of the 400-km transition remains fairly constant at about 70 K, because latent heat production is in equilibrium with thermal diffusion. After 15 Ma, the slab is attracted by the 400-km transition, neighboring mantle material is accelerated downwards and the effects of latent heat again dominates thermal diffusion. The effects of the accelerating slab motion on the 670-km transition is less direct and not clearly observable in Fig. 3a,b.

The robustness of the latent heat effects is tested through variation of several model parameters. As an indicator of the latent heat effect, we estimated the length of the flat slab segment below the overriding continent. The horizontal position of the point of penetration of the slab through the 400-km transition was used to quan-

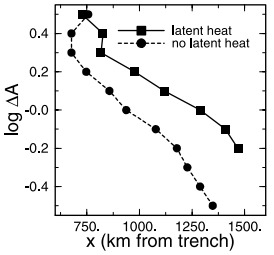

Fig. 4. Relation between the length of the flat slab segment and mantle viscosity prefactor A, relative to the reference values in Table 1, for models with (solid line) and without (dashed line) latent heat. The prefactor A and the effective mantle viscosity are inversely related (see text). The x-axis displays the horizontal distance between trench and slab breakthrough point. The length of the flat slab segment increases with effective mantle viscosity with approximately 600 km in the case without latent heat. The effects of latent heat results in an extra 150–300 km of flat-lying slab segment.

tify this segment length. The importance of trench migration and the mantle viscosity on ability of the slab to penetrate into the lower mantle has been shown by [22,23]. In previous work we have shown that mantle viscosity is also a key parameter for the occurrence of shallow flattening of the slab at a depth of about 100 km [9]: during a trenchward motion of the overriding plate, a strong mantle resists steep Benioff type subduction. Furthermore, viscosity controls the interaction between vertical slab motion and flux of mantle material through the 400-km transition. We varied the effective mantle viscosity through variation of the viscosity prefactors A in Eq. 7, around the reference values from Table 1, of both the diffusion and dislocation creep components of the composite rheology. The relationship between A and the effective viscosity η is dependent on the local circumstances for a composite rheology [9]: with the rheological parameters from Table 1, a one order-of-magnitude decrease of A results in an effective viscosity increase with a factor between 2 and 10. Fig. 4 shows the effect of the prefactor variation ΔA with respect to the reference model on the horizontal position of the point of slab penetration through the 400-km phase transition. A positive correlation between effective mantle viscosity and the length of the flat slab segment is observed for models with and without latent heat. Latent heat increases the flat slab length by approximately 150 km in a weak mantle, and up to 300 km in a stronger mantle. Only the models with the weakest mantle do not show this feature. No real flat slab segment occurs in the models with a low-viscosity mantle, and in this case a reduction of the subduction angle is a better description of the latent heat effect. Besides a buoyancy effect, the thermal anomaly also influences the temperature-dependent mantle viscosity near the phase transitions. Although this weakening may be as large as half an order-of-magnitude just below the 400-km transition, the surface area of this phenomenon is too small to have a significant influence on the dynamics. On the whole, the importance of the mantle viscosity in these models is quite remarkable: the style of subduction changes from steep Benioff type subduction to flat subduction with a flat slab segment length of about 1000 km by changing the mantle viscosity with less than one order-of-magnitude, which is well within the uncertainty of estimates of effective upper mantle viscosity [24].

In the scenario of lithospheric doubling, the occurrence of flat subduction is mainly due to the overriding continent [9,22,23]. Therefore, we varied the velocity of the overriding continent with respect to the deep mantle. Fig. 5 illustrates the effect of the varying overriding velocity v_{ov} on the lateral position of the breakthrough point.

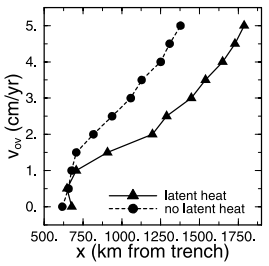

Fig. 5. Effect of the overriding velocity on the length of the flat slab segment for models with (solid line) and without (dashed line) latent heat. The horizontal axis shows the horizontal distance between trench and slab breakthrough point. Steep subduction occurs for a low continental overriding velocity (<1.5 cm/yr). A higher overriding velocity leads to an increasing slab length. Latent heat results in no extension of the flat slab segment for an overriding velocity of 1 cm/yr or less, up to a fairly constant extra flat slab length of about 400 km for an overriding velocity of 3 cm/yr or more.

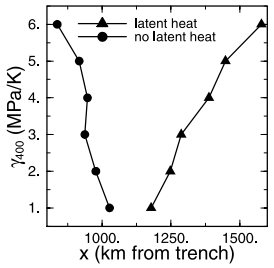

Fig. 6. The relation between Clapeyron slope of the 400-km phase transition and the length of the flat slab segment. The horizontal axis shows the horizontal distance between trench and slab breakthrough point. In case of latent heat (triangles), the flat slab grows roughly linearly with increasing Clapeyron slope. Without latent heat (circles), a stronger transition pulls down the slab more firmly, resulting in a shorter flat slab.

Steep subduction occurs in case of no or a small overriding velocity and latent heat seems to make little difference in these cases. When the overriding velocity exceeds approximately 1.5 cm/yr, the slab starts to flatten: the slab penetrates the 400-km transition further away from the trench. The length of the flat slab segment increases monotonically with increasing overriding velocity. With the flattening, the effect of latent heat release becomes increasingly important. For an overriding velocity of 3 cm/yr or higher, the effect of latent heat release leads to a slightly growing increase of the length of the flat slab segment to a little more than 400 km. This figure shows that the effectiveness of the latent heat release is not directly depending on the overriding velocity, but only indirectly through the style of subduction (high- or low-angle subduction).

Finally, we varied the strength of the 400-km phase transition through variation of the Clapeyron slope between 1 and 6 MPa/K, which affects the amount of latent heat release (Eq. 1). As shown in Fig. 3, the effects of the 670-km transition are relatively small. We kept the parameters of this transition constant during the experiments to extract the influence of the greater impact of the 400-km phase transition. Fig. 6 shows the effects of varying the Clapeyron slope on the lateral position of the breakthrough point. A roughly linear relation is present between the Clapeyron slope and the horizontal extent of the flat slab. Changing the Clapeyron slope from 1 to 6 MPa/K results in an extra 400-km flat slab segment. This is the result of two effects: on the one hand, once the slab reaches the vicinity of the phase transition, a strong transition tends to pull the slab more firmly, resulting in a shorter flat slab segment, which is visible from the results of experiments without latent heat. On the other hand, more latent heat release of the stronger transition leads to a stronger resisting buoyancy opposing penetration of the flat slab. The latter effect dominates, as illustrated with the curve of experiments with latent heat.

5. Discussion and concluding remarks

Shallow or very low-angle subduction is occurring at about 10% of the modern subduction zones [7]. As an explanation for this feature, the effect of the trenchward moving overriding plate [8,9] has been proposed. We have investigated the effects of latent heat of the mantle phase transitions at 400 and 670 km depth on the dynamics of low-angle subduction below a trenchward moving overriding continent. In such a situation, an overriding continent forces an oceanic plate to subduct to at least 100 km depth. This, in turn, pushes underlying mantle material down through the phase transitions, where latent heat release or absorption gives rise to positive phase buoyancy. For the 400-km transition, the maximum temperature change and depression are approximately 80 K and 8 km, respectively, while for the 670-km transition these are only 20 K and 2 km, respectively. We examined the significance of these latent heat effects on the dynamics of the slab. A 32-Ma-old slab, which is forced to subduct into a moderately strong mantle below an overriding continent with 2.5 cm/yr, travels horizontally approximately 350 km further and 11 Ma longer if latent heat is included in the model calculations. As shown here, rapid vertical motion through the phase transitions results in a temperature discontinuity across the transition due to latent heat, which diffuses away again with time. Our initial temperature profile assumes no effects of latent heat release. This is a good assumption in case

of a trenchward moving overriding plate, which continuously forces a different part of the mantle to sink through the phase transitions.

The style of subduction is strongly dependent on the mantle viscosity: a viscosity increase of only one order-of-magnitude may change the style of subduction from steep to horizontal. The significance of latent heat does not change much within this range. Variation of the overriding velocity changes the style of subduction from steep, for an overriding velocity of 1 cm/yr or less, to flat subduction, when the overriding velocity exceeds 3 cm/yr. Effects of latent heat are negligible at low overriding velocity, and show a slightly growing flat slab length increase to about 400 km above 3 cm/yr overriding velocity. The relation between the Clapeyron slope and the length of the flat slab is almost linear. An increase of γ from 1 to 6 MPa/K leads to a 400-km-longer flat slab segment. These results indicate that buoyancy effects from latent heat at low-angle subduction below an overriding continent form a robust feature that increases the tendency to flat subduction significantly.

Acknowledgements

The authors would like to thank Bertram Schott for helpful discussions and Greg Houseman for a constructive review. This work was sponsored by the Stichting Nationale Computerfaciliteiten (National Computing Facilities Foundation, NCF) for the use of supercomputer facilities, with financial support from the Nederlandse Organisatie voor Wetenschappelijk Onderzoek (Netherlands Organization for Scientific Research, NWO). *[RV]*

References

[1] D.L. Turcotte, G. Schubert, Geodynamics, Applications of Continuum Physics to Geological Problems, John Wiley and Sons, New York, 1982.
[2] U.R. Christensen, D.A. Yuen, Layered convection induced by phase transitions, J. Geophys. Res. 99 (1985) 10291–10300.
[3] P.J. Tackley, D.J. Stevenson, G.A. Glatzmaier, G. Schubert, Effects of multiple phase transitions in a three-dimensional spherical model of convection in Earth's mantle, J. Geophys. Res. 99 (1994) 15877–15901.
[4] M.R. Riedel, S. Karato, Grain-size evolution in subducted oceanic lithosphere associated with the olivine–spinel transformation and its effects on rheology, Earth Planet. Sci. Lett. 148 (1997) 27–44.
[5] H. Schmeling, R. Monz, D.C. Rubie, The influence of olivine metastability on the dynamics of subduction, Earth Planet. Sci. Lett. 165 (1999) 55–66.
[6] M.J.R. Wortel, N.J. Vlaar, Age-dependent subduction of oceanic lithosphere beneath western South America, Phys. Earth Planet. Inter. 17 (1978) 201–208.
[7] M.-A. Gutscher, W. Spakman, H. Bijwaard, E. Engdahl, Geodynamics of flat subduction seismicity and tomographic constraints from the Andean margin, Tectonics 19 (2000) 814–833.
[8] N.J. Vlaar, Thermal anomalies and magmatism due to lithospheric doubling and shifting, Earth Planet. Sci. Lett. 65 (1983) 322.
[9] J. van Hunen, A.P. van den Berg, N.J. Vlaar, A thermomechanical model of horizontal subduction below an overriding plate, Earth Planet. Sci. Lett. 182 (2000) 157–169.
[10] U.R. Christensen, Dynamic phase boundary topography by latent heat effects, Earth Planet. Sci. Lett. 154 (1998) 295–306.
[11] C. Bina, G. Helffrich, Phase transition clapeyron slopes and transition zone seismic discontinuity topography, J. Geophys. Res. 99 (1994) 15853–15860.
[12] J. Ita, S.D. King, Sensitivity of convection with an endothermic phase change to the form of governing equations, initial conditions, boundary conditions, and equation of state, J. Geophys. Res. 99 (1994) 15919–15938.
[13] S.H. Kirby, S. Stein, E.A. Okal, D.C. Rubie, Metastable mantle phase transformations and deep earthquakes in subducting oceanic lithosphere, Rev. Geophys. 34 (1996) 261–306.
[14] G. Segal, N.P. Praagman, The sepran package, Tech. rep., http://dutita0.twi.tudelft.nl/sepran/sepran.html, 2000.
[15] A.P. van den Berg, P.E. van Keken, D.A. Yuen, The effects of a composite non-Newtonian and Newtonian rheology on mantle convection, Geophys. J. Int. 115 (1993) 62–78.
[16] A.P. van den Berg, D.A. Yuen, Is the lower-mantle rheology Newtonian today?, Geophys. Res. Lett. 23 (1996) 2033–2036.
[17] B. Schott, H. Schmeling, Delamination and detachment of a lithospheric root, Tectonophysics 296 (1998) 225–247.
[18] R. Trompert, U. Hansen, Mantle convection simulations with rheologies that generate plate-like behaviour, Nature 395 (1998) 686–689.
[19] G.A. Abers, Hydrated subducted crust at 100–250 km depth, Earth Planet. Sci. Lett. 176 (2000) 323–330.
[20] S. Peacock, R. Hyndman, Hydrous minerals in the mantle wedge and the maximum depth of subduction thrust earthquakes, Geophys. Res. Lett. 26 (1999) 2517–2520.

[21] H.M. Benz, J.E. Vidale, Sharpness of upper-mantle discontinuities determined from high-frequency reflections, Nature 365 (1993) 147–150.
[22] U.R. Christensen, The influence of trench migration on slab penetration into the lower mantle, Earth Planet. Sci. Lett. 140 (1996) 27–39.
[23] D. Olbertz, M.J.R. Wortel, U. Hansen, Trench migration and subduction zone geometry, Geophys. Res. Lett. 24 (1997) 221–224.
[24] K. Lambeck, P. Johnston, The viscosity of the mantle: Evidence from analysis of glacial-rebound phenomena, in: The Earth's Mantle: Composition, Structure and Evolution, Cambridge University Press, Cambridge, 1998, pp. 461–502.
[25] S. Karato, P. Wu, Rheology of the upper mantle a synthesis, Science 260 (1993) 771–778.
[26] G. Shelton, J. Tullis, Experimental flow laws for crustal rocks, EOS Trans. Am. Geophys. Union 62 (1981) 396.
[27] S. Karato, D.C. Rubie, Toward an experimental study of deep mantle rheology: A new multianvil sample assembly for deformation studies under high pressures and temperatures, J. Geophys. Res. 102 (1997) 20111–20122.
[28] V. Steinbach, D.A. Yuen, The effects of temperature-dependent viscosity on mantle convection with two major phase transitions, Phys. Earth Planet. Inter. 90 (1995) 13–36.